

See discussions, stats, and author profiles for this publication at: <https://www.researchgate.net/publication/308709141>

Materials Testing of 3D Printed ABS and PLA Samples to Guide Mechanical Design

Conference Paper · June 2016

DOI: 10.1115/MSEC2016-8668

CITATIONS

23

READS

15,183

2 authors:



Daniel Farbman

1 PUBLICATION 23 CITATIONS

SEE PROFILE



Chris D. McCoy

University of California, Berkeley

10 PUBLICATIONS 41 CITATIONS

SEE PROFILE

Some of the authors of this publication are also working on these related projects:



Berkeley Micromechanical Analysis and Design [View project](#)



Hands-on Rapid Prototyping [View project](#)

MSEC2016-8668

MATERIALS TESTING OF 3D PRINTED ABS AND PLA SAMPLES TO GUIDE MECHANICAL DESIGN

Daniel Farbman

University of California, Berkeley
Berkeley, California, United States of America

Dr. Chris McCoy

University of California, Berkeley
Berkeley, California, United States of America

ABSTRACT

A set of monotonic tensile tests was performed on 3-D printed plastics following ASTM standards. The experiment tested a total of 13 “dog bone” test specimens where the material, infill percentage, infill geometry, load orientation, and strain rate were varied. Strength-to-weight ratios of the various infill geometries were compared. It was found through tensile testing that the specific ultimate tensile strength (MPa/g) decreases as the infill percentage decreases and that hexagonal pattern infill geometry was stronger and stiffer than rectilinear infill. However, in finite element analysis, rectilinear infill showed less deformation than hexagonal infill when the same load was applied. Some design guidelines and future work are presented.

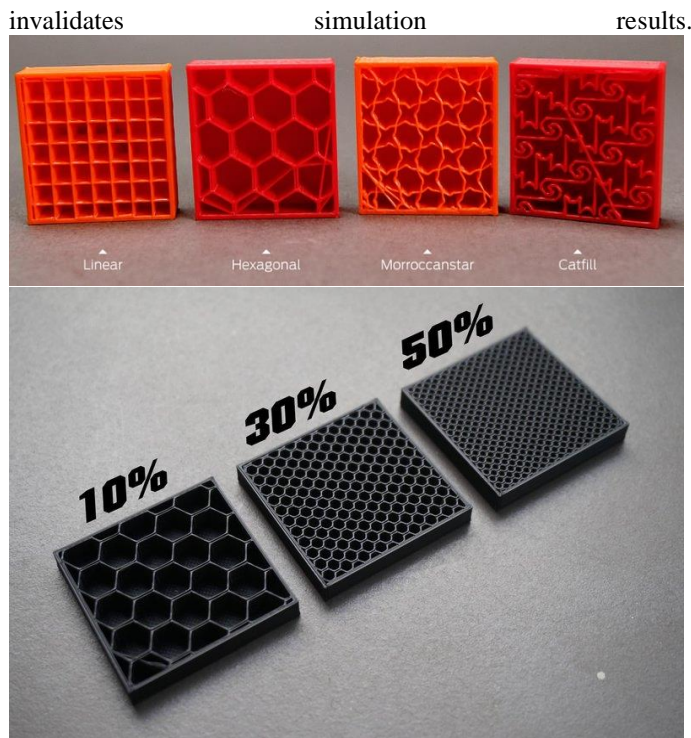
Glass Transition	221°F (105°C)	140-149°F (60-65°C)
Tensile Strength	6,500 psi (44.81 MPa)	8,383.18 psi (57.8 MPa)
Flexural Strength	11,000 psi (75.84 MPa)	8,020.58 psi (55.3 MPa)
Tensile Modulus	320,000 psi (2.21 GPa)	478,624.53 psi (3.3 GPa)
Flexural Modulus	330,000 psi (2.28 GPa)	333,586.79 psi (2.3 GPa)

Table 1: Mechanical properties of both tested plastics [1].

INTRODUCTION

The increased use of 3D printing as a learning tool and to generate functional end-use parts have generated the need for a better understanding of the mechanical behavior of 3D printed parts and the development of analytical tools and design guidelines for engineers. Materials testing of 3D printed plastics was performed in order to provide both industrial and academic communities with new to improve mechanical and digital design in the context of additive manufacturing; specifically fused deposition modeling (FDM). Mechanical engineering design and education has traditionally focused on the use and study of isotropic materials (uniform mechanical behavior and material characteristics in all directions) which are typically easier to analyze, procure, and manufacture. This is, in part, due to the fact that many engineering materials such as metals and thermoset plastics can be approximated as isotropic. However, 3D printers often generate parts that are modeled as solid objects in CAD software, but when fabricated, the shapes include user-specific *infill geometries* which replace the solid internal volume with a more material efficient, structural lattice known as *infill*. These infill geometries are generated by proprietary or open-source *slicing algorithms* and are utilized to generate the numerical code or gcode necessary to manufacture using consumer-grade 3D printers, but unless deliberately accounted for in the CAD model, transform the geometry and thereby

	ABS <i>Acrylonitrile butadiene styrene</i>	PLA <i>Poly(lactic acid) or polylactide</i>
Molecular Formula	(C ₈ H ₈ ·C ₄ H ₆ ·C ₃ H ₃ N) _n	(C ₃ H ₄ O ₂) _n
Environmentally Friendly?	NO	YES
Degradable?	NO	YES
Melting Point	205°C	175°C
Rockwell Hardness	R105 to R110	R70 to R90
Surface Quality	Fine	Good
Cool Time	Medium	Long
Moisture Absorption	Approx. 3%-5%	Minor
Density	1.04 g/cm ³	1.23 to 1.25 g/cm ³
Elongation at Break	20%	3.8%



Figures 1 [6] and 2 [8]: Photos of 3D parts printed without an upper shell to illustrate concepts of infill geometry and infill percentage. Thickness of the walls, infill geometry and the infill percentage (converted to adjusting the size of the geometric features) are specified in a print command.

3D printers are designed to print parts in this way for several important reasons. The strength to weight ratio may be improved with material only in certain key locations which are most important for the structural integrity of the material. Also the part is lighter. Lower mass is usually a benefit in and of itself, but the production cost is reduced, as less material is required to produce the part, which is always beneficial, and the part prints much faster (from experimentation, print time is close to directly proportional to volume for many objects). Standard infill percentages are 10%-25% meaning that a part with an infill structure could print in approximately one fourth the time of a fully solid part.

3D printers are designed to print parts in this way for several important reasons. The major reason is that 3D printing is slow (~80 mm/s print speeds, which translates to ~1 hour per cubic inch at 15% infill) and thus, the less material the machine needs to use in order to generate a part, the faster the machine prints (assuming no print failures). Additionally, beyond just faster print times, often design requirements have weight strength-to-weight specifications which benefit from less material extrusion. Less material consumption is often more advantageous from cost and environmental perspectives and when designing for technical applications, one would want to choose their infill geometry, infill percentage, and part orientation intelligently. However, modeling every designed part with every infill

geometry, orientation and percentage and performing analysis on such models is difficult and time consuming. If a set of "Design for Digital Fabrication" guidelines existed, which were based on a sound engineering analysis and coupled with world-class experimental results--people who generate designs for these tools will improve not only their own capabilities but any other stakeholder who participates in the design and fabrication of physical parts. The results of this research would help to construct those guidelines.

Even if a CAD tool added a feature to automatically generate an infill for a solid part, the computational analysis of that part with the finite element method would have additional challenges. Infill geometry makes the domain incredibly complex and strains the algorithms which drive the finite element solutions. The number of elements in a part STL file that includes infill geometry increases the number of elements by one to two orders of magnitude depending on the complexity of such geometry (as observed from prior Solidworks experimentation and experience). This would cause a drastic increase in the computational power necessary to analyze such a model as well as analysis time--during a phase of product development where time is of the essence ("rapid prototyping"). Also, a domain with smaller elements could cause the finite element algorithm to diverge numerically resulting in a failed analysis.

BACKGROUND

Research has also shown that the material properties of ABS 3D printer plastic are affected by the 3D printer process and that the bulk material is anisotropic in nature [2]. Therefore, if infill material had different orientations relative to other infill material, then the strength of such a design could not be predicted.

Previous experimentation has focused primarily on print orientation for solid parts and infill variation for parts which use infill. This experiment looks at the interplay of both these factors. Also, effects of infill density, which this experiment addresses, have not been thoroughly examined

The goal of this experiment is to provide designers with an essential set of design guidelines based on experimentally obtained data and insights that they can rely on when designing mechanical parts. This will enable designers to make better 3D modeling and design choices without requiring time-consuming and complex analysis when leveraging additive manufacturing for rapid prototyping.

METHODOLOGY

The experiment consisted of monotonic tensile tests to fracture of test specimens using the Instron tensile testing machine with different infill geometries and infill geometry origins to extract and compare the mechanical properties of each.

In order to test the various infill geometries and orientations it was necessary to define them in a coordinate system related to the standard tensile test specimen. To that end, a set of axes were defined for all test specimens. These were the length, width and

thickness axes whose orientation relative to a test specimen is shown in the figure.

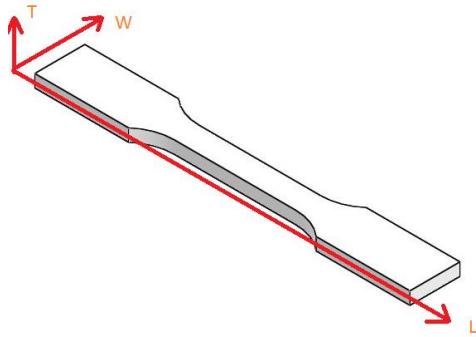


Figure 3: CAD of sample with orientation axis L, W, and T (length, width, and thickness) labeled.

Each infill geometry is described by the geometric shape which is repeated throughout the interior of the object. These geometric shapes are perpendicular to the print axis. Each geometric shape has multiple main axes with names based on their orientation relative to the geometric shape. These are listed below.

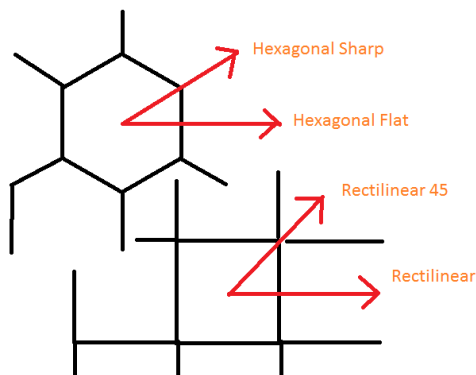


Figure 4: The infill geometries with main axis labeled. The tensile force is always aligned with the main axis of the orientation.

The plane perpendicular to the print axis is labeled with the pair of axes which define it. The first letter of the label is the axes which is parallel to the main axis of the infill geometry.

The strength of each sample was found by performing a monotonic tensile test on it. In a monotonic tensile test as defined by ASTM code B557-06 [5] dog-bone like test specimens (pictured in figure 3) are stretched at a fixed speed until they fracture. The samples were produced using a desktop 3D printer employing the program “Repetier” to convert the stl file of the standard test specimen created using Solidworks and to control the infill geometry properties.

This set of tests was performed in an Instron testing apparatus. The specimens are designed such that the ends which grip onto the clamps in the Instron testing apparatus are wider and therefore stronger than the rest of the specimen. The center

part of the specimen does not change in width. This is referred to as the gauge length or testing region and is the only region of interest to the test. Since the ends of the test specimen are clamped into place and they are much stiffer than the rest of the specimen it is assumed that any length change would happen in the testing region. Length, width, and thickness of the testing region are entered into the program Bluehill 3 which controls the Instron test.

Force versus percent elongation is recorded every tenth of a second during the test which stops immediately after fracture. After the test, Force (F) is converted to (engineering) stress (σ) by dividing it by the cross-sectional area (A) of the testing region (thickness (t) times width (w)) ($\sigma = \frac{F}{A} = \frac{F}{t \cdot w}$). (Engineering) strain (ϵ) is found by dividing percent elongation by 100. (Strain is defined as change in length divided by the original length).

From the stress-strain curve two measures are obtained. The first is the ultimate tensile strength of the specimen. This is the highest stress measure obtained and represents the highest stress it can withstand without breaking. For relatively small loads the bulk material can be approximated as a spring in which displacement is directly proportional to force. Therefore, stress is directly proportional to strain. This constant of proportionality between stress and strain is called the Young's modulus (E) and measures the stiffness of the material. ($\sigma = E \cdot \epsilon$) For this test lines were fit to all specimens' stress-strain curves in the same displacement range of 0.5 to 1.5 mm. The slope of the line fit to the data in that region is the Young's modulus. The R^2 values for all lines were larger than .97 indicating an incredibly good fit. Whether or not the fits would be good was uncertain prior to testing due to the fact that most test specimens were not solid.

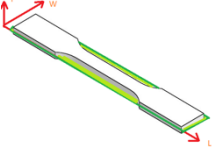
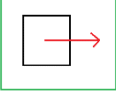
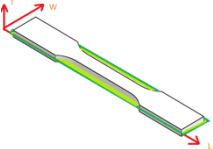
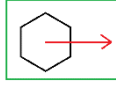
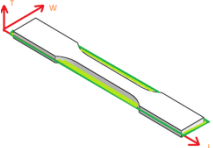
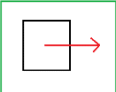
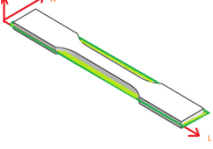
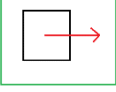
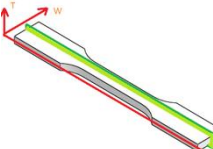
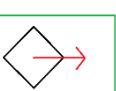
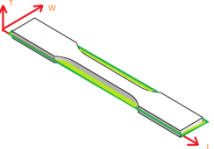
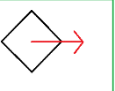
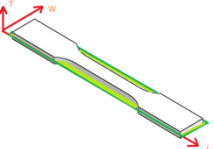
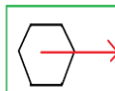
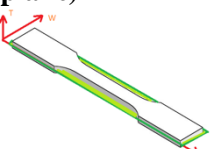

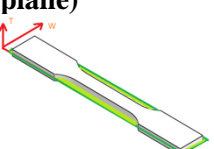
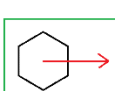
Some orientations were tested a faster strain rate. Experimental data shows that plastic becomes stiffer when strained at a higher strain rate. Due to the complex nature of the infill geometry, it was hypothesized that the geometries may not have the same behaviors that they have at slower strain rates meaning that the best geometry for more dynamic loads may be different than the best geometry for relatively static loads.

Humidity and temperature were also monitored using an Acurite brand indoor humidity and temperature monitor, although due to the limited absorptivity of the material and the fact that the glass transition is at such a high temperature [1] and it was found that the temperature and humidity levels were well controlled. Therefore the effects of both were assumed be small enough not to invalidate the experimental finding.

RESULTS

Tensile Test Results

The results of the tensile tests were in the form of force versus percent elongation curves, which were converted into stress-strain curves. From those curves a Young's Modulus and ultimate tensile strength were extracted for each test specimen.

Infill Orientation	Geometry	+	Fracture Notes
1. Rectilinear (l-w plane)	 		
2. Hexagonal Flat (l-w plane)	 		Failed near end of gauge length
3. Rectilinear (l-w plane)	 		
4. Rectilinear (l-w plane)	 		Failed near end of gauge length
5. Rectilinear 45 (l-t plane)	 		Failed near end of gauge length
6. Rectilinear 45 (l-w plane)	 		
7. Hexagonal Sharp (l-w plane)	 		
8. Shell			Failed near end of gauge length
9. Solid			
10. Hexagonal Sharp (l-w plane)	 		
11. Shell			Failed Outside Gauge length
12. Hexagonal Flat (l-w plane)	 		Failed Outside Gauge length

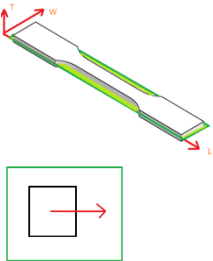
13. Rectilinear (l-w plane) 	Failed near visible surface damage
---	------------------------------------

Table 2: Tensile test results for the monotonic tensile tests performed. Notes about failure are presented as many test specimens did not fail at or near the center of the gauge length. Cross-sections of each infill type are depicted as a visual reference.

#	% Infill	$\dot{\epsilon}$ (mm/min)	E (MPa)	UTS (MPa)
1	20	15	594.9	20.22
2	20	15	635.3	19.81
3	20	6	450.5	17.68
4*	20	15	494.9	16.60
5	20	3	546.5	17.30
6	15	3	422.4	15.31
7	15	3	561.6	20.07
8	0	3	370.3	13.21
9	100	3	973.0	46.18
10	15	3	620.0	21.57
11	0	3	646.1	19.56
12	15	3	591.1	21.48
13	15	3	478.6	13.59

Table 3: Tensile test results for the monotonic tensile tests performed. (strain rate, Young's modulus, and ultimate tensile strength). All specimens were made of PLA except for number 4 which was carbon fiber PLA proto-pasta.

#	Infill Geo. + Orient.	% Infill	Mass (g)	Max Force (N)	SR*	ISR*
1	Rectilinear (l-w plane)	20	11.535	1574.099	0.926	1.065
2	Hexagonal Flat (l-w plane)	20	13.327	1562.489	0.6	0.630
3	Rectilinear (l-w plane)	20	11.765	1451.819	0.838	0.722
4	Rectilinear (l-w plane)	20	10.782	1291.768	0.813	0.564

5	Rectilinear 45 (l-t plane)	20	14.496	1479.604	0.693	0.409
6	Rectilinear 45 (l-w plane)	15	12.500	1332.241	0.724	0.374
7	Hexagonal Sharp (l-w plane)	15	14.564	1672.405	0.780	0.617
8	Shell	0	8.768	1114.584	0.863	N/A
9	Solid	100	29.212	4302.964	1 (def.)	1 (def.)
10	Hexagonal Sharp (l-w plane)	15	16.355	1865.497	0.774	0.635
11	Shell	0	15.442	1695.266	0.745	0.558
12	Hexagonal Flat (l-w plane)	15	15.586	1863.187	0.812	0.704
13	Rectilinear (l-w plane)	15	10.894	1026.764	0.640	-0.265

Table 4: Shows the strength increase caused by each infill relative to its mass. This is compared to that of the solid infill by defining its strength ratio as 1. *See equations 1 and 2.

$$\text{Strength Ratio (SR)} \stackrel{\text{def}}{=} \frac{F_{\max} / \text{mass}}{F_{\max, \text{solid}} / \text{mass}_{\text{solid}}}$$

Equation 1: Definition of the "strength ratio" in this analysis. This is used to see how the various infill styles affect the strength to mass ratio of the sample. The subscript "solid" refers to sample 9 which was completely solid.

$$\text{"Increase in Strength" Ratio (ISR)} \stackrel{\text{def}}{=} \frac{F_{\max} - F_{\max, \text{shell}} / \text{mass} - \text{mass}_{\text{shell}}}{F_{\max, \text{solid}} - F_{\max, \text{shell}} / \text{mass}_{\text{solid}} - \text{mass}_{\text{shell}}}$$

Equation 2: Definition of the "Increase in strength" ratio in this analysis. This is used to see how the various infills changed the strength of the sample from a hollow shell. Subscript "shell" refers to sample 8 which was a hollow shell. The subscript "solid" refers to sample 9 which was completely solid.

These equations are unconventional in their comparison of maximum forces as opposed to stresses. This was done because the specimens had dissimilar cross-sections making a comparison of stress to mass ratios invalid. Suppose we had a test specimen of 6060 aluminum of uniform density which behaved ideally. It would have thickness "t", cross-sectional area "A", engineering ultimate tensile strength "U", mass "m" and a maximum force exerted in a tensile test equal to "F". Therefore, $U = \frac{F}{A}$. Define R as the ratio between the engineering ultimate tensile strength and the mass. So, for this specimen, $R = \frac{U}{m}$. Suppose we had a second specimen of the same material which also had uniform density and behaved ideally. However, suppose this specimen had a thickness $c * t$ with c being a constant larger than 1 and all other dimensions were the same. In this case the mass would now be $c * m$ and the area would be $c * A$. However, since the two specimens are of the same material, U would remain unchanged. The maximum force would therefore be equal to cF . ($U = \frac{F}{A} = \frac{c * F}{c * A}$). This would cause R to become: $\frac{U}{c * m}$. If R was used as a means of comparison, two specimens with identical material properties would be assessed as having different strength to mass ratios. However, the strength ratio used for comparison in equation 1 would give identical values for both specimens. $\frac{F}{m} = \frac{c * F}{c * m}$

Ideally, the comparison would be made using an ultimate tensile strength to density ratio, however density data was not taken.

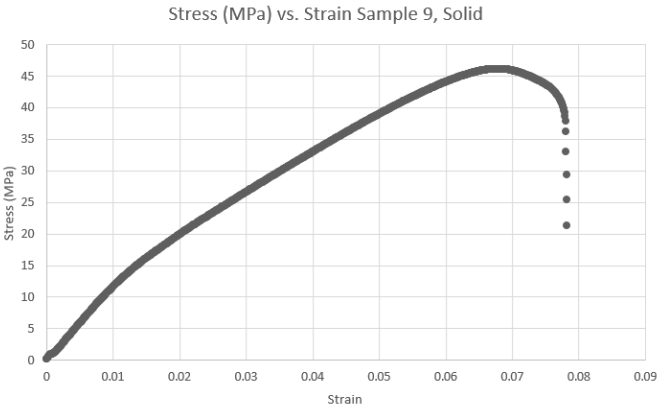


Figure 5: Stress versus strain for sample 9, solid.

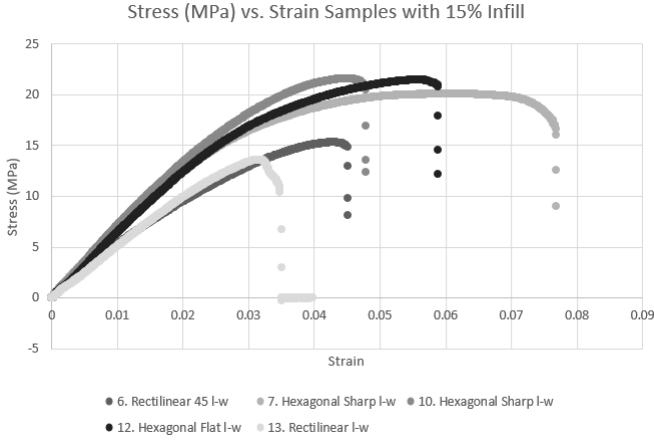


Figure 6: Stress versus strain for samples with 15% infill.

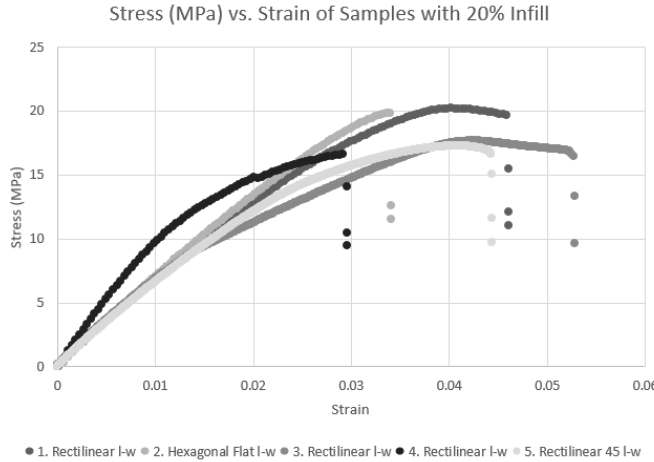


Figure 7: Stress versus strain for samples with 20% infill.

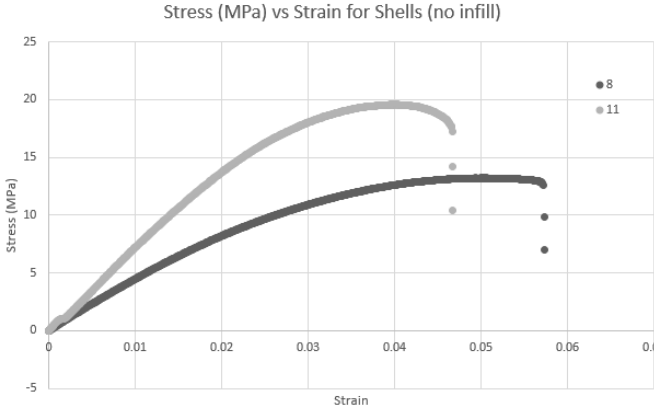
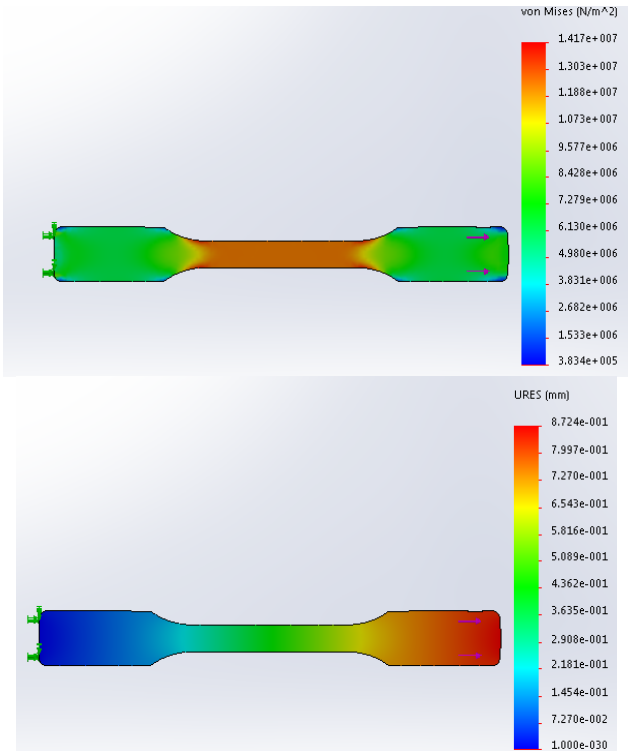


Figure 8: Stress versus strain for samples with 15% infill.

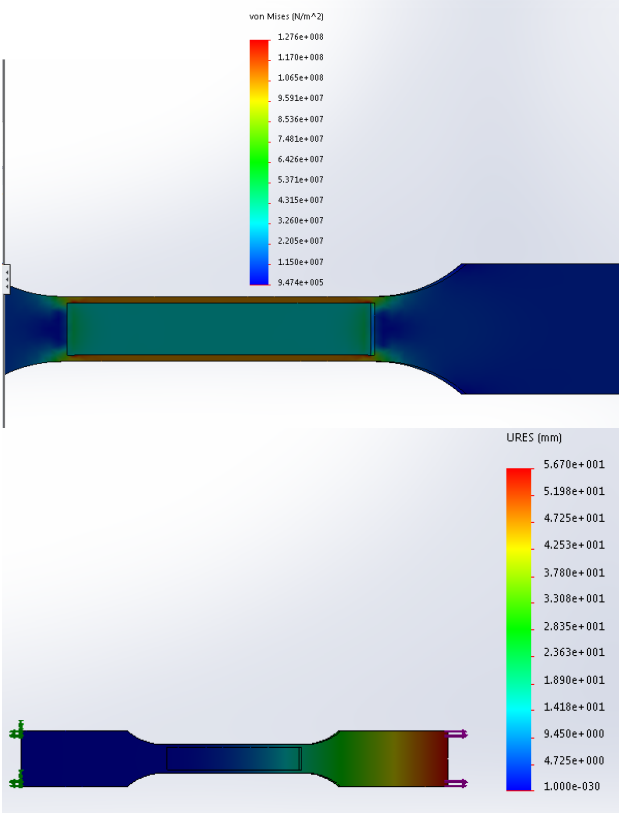
Finite Element Analysis Results

The finite element analysis consisted of four stress simulations in which a tensile load of 1000 N was applied to CADs of test specimens. In all simulations, one face in the thickness-width plane was fixed and a uniformly distributed load of 1000 N was applied to the face on the other side. These consisted of a solid specimen, a hollow specimen, a rectilinear specimen (Rectilinear 45 l-w plane), and a hexagonal specimen

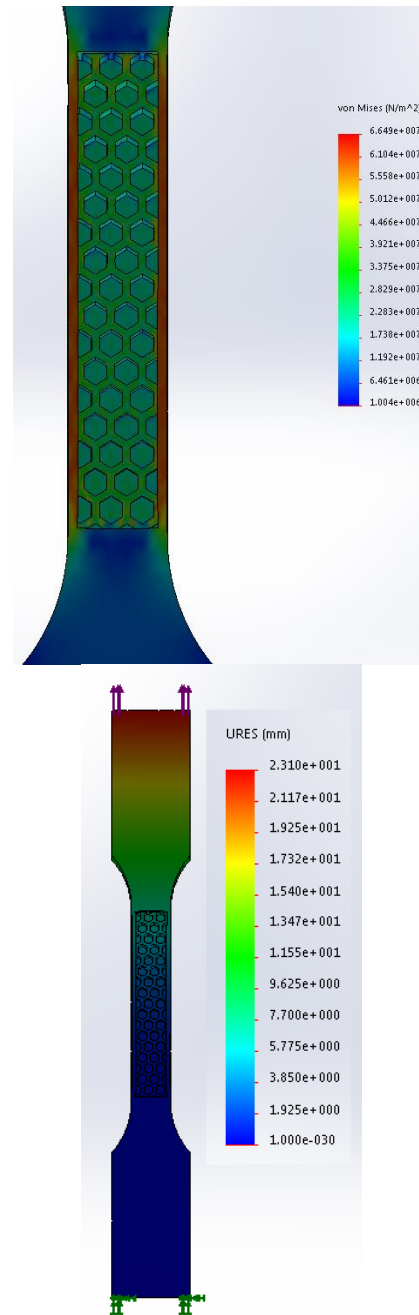
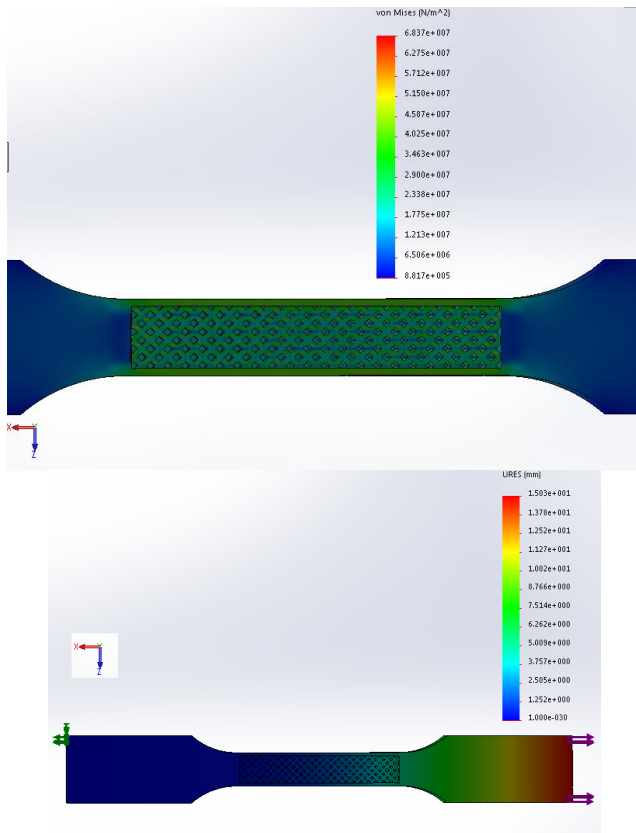
(Hexagonal Sharp l-w plane). Both the rectilinear and hexagonal specimens had infill percentages of 25% and infill geometry thickness of 1mm. All specimens had exterior wall thicknesses of 1.2mm and the volume outside the gauge length was solid.



Figures 9 and 10: Simulated stress and displacement responses of a solid sample to a 1000 N load. The maximum deformation is 0.8724 mm, a strain of 0.014. Stresses are reported in Pascals.



Figures 11 and 12: Simulated stress and displacement responses of a sample with only a shell along the gauge length to a 1000 N load (12.0 MPa stress). The top shell is not shown so internal stresses are visible. The maximum deformation is 56.70 mm, a strain of 0.92. Stresses are reported in Pascals.



Figures 13 and 14: Simulated stress and displacement responses of a sample with rectilinear infill and a shell around the infill along the gauge length to a 1000 N load (12.0 MPa stress). The top shell is not shown so internal stresses are visible. The maximum deformation is 15.03 mm, a strain of 0.24. Stresses are reported in Pascals. This is quite similar to specimen 6 at that point (error < 5%)

Figures 15 and 16: Simulated stress and displacement responses of a sample with hexagonal infill and a shell around the infill along the gauge length to a 1000 N load (12.0 MPa stress). The top shell is not shown so internal stresses are visible. The maximum deformation is 23.10 mm, a strain of .37. Stresses are reported in Pascals. The stress (12 MPa) differs greatly from the values of specimens 7 and 10 (hexagonal sharp, l-w, 15% infill) at that strain (~17 and ~20 MPa).

DISCUSSION

Interpretations based on the data

Of the samples which were stressed at 3mm/min, the samples with hexagonal infill had significantly higher ultimate tensile strengths than rectilinear samples. Some samples were stressed at a faster strain rate. This was in attempt to find a strain rate which was a reasonable approximation of a static load and that could be used for a relatively fast test. It was observed that elongating a sample at 3 mm/min produced a similar tensile strength to elongating one at 6mm/min and that it allowed for a short test of just under two minutes. Therefore, the elongation rate of 3 mm/min was used for all subsequent samples. Sample 1 was elongated at 15 mm/min and Sample 3 was elongated at 6 mm/min. Both had identical infill. Sample 1 was 32.1% stiffer and had an ultimate tensile strength 14.4% larger. This indicates that just like with most solid materials, 3D printed parts become stiffer at faster strain rates.

An examination of strength to mass ratios was performed. It was hypothesized that the use of infill would increase the strength-to-mass ratio however, the results indicate that parts with lower infill percentages have lower strength to mass ratios. Also, on average, parts with hexagonal infill were stronger and stiffer than those with rectilinear infill and the strength of parts with hexagonal infill was more consistent as a function of orientation. ("Rectilinear 45" had lower ratios than "Rectilinear".)

The finite element analysis indicated that specimens with rectilinear infill would be stiffer than those with hexagonal infill. However, the opposite was shown in experimentation. Also, the results for the finite element analysis of the rectilinear test specimen more closely matched the experimental results for the test specimens with the same infill geometry. This discrepancy may be due in part to anisometry in the strength of the infill. The printing process may have changed the properties of the hexagonal infill in such a way as to invalidate computer simulation using uniform material properties.

Error Sources and Their Consequences

- Major printing errors

Many printed samples were not printed to specification. Some samples had large lumps of printing material stuck to them which had to be removed with a belt sander so they could fit into the Instron machine. Also the top wall of sample 13 was missing and it fractured near a large surface crack approximately 2-3 mm long. This made some samples fracture prematurely. Therefore their ultimate tensile strengths were seen as lower than they

would have been with a sample that was perfectly to specification.

- Failure outside of gauge length

Many factors contributed to some samples falling outside the gauge length. Besides the printing errors mentioned above, the hexagonal sample with 15% infill had geometry which was larger than the width of the area of the test specimen in the gauge length.

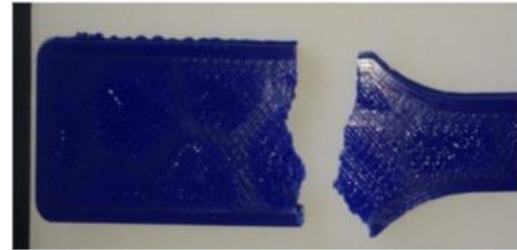


Figure 17: A photo of the fracture of sample 12. This sample failed outside the gauge length along a line with little infill

- Approximation of uniformity

Assuming that the specimens and their properties could be approximated as uniform even though they were not fully solid was a fundamental assumption of this (and any) tensile test. Properties are assumed to be uniform along the gauge length. This is what gives the stress and strain measures their meaning. This was more of an approximation than an assumption in the case of specimens with infill geometry that are not fully solid. Also, in order to make specimens which held up to testing, we had to give them exterior walls. These shells around the infill contribute to the strength of the specimens even though the focus should be on the infill strength versus the solid strength. The gauge length of the specimens had a rectangular cross section of about 13mm by 6.4mm making walls that were about 0.8 mm thick constitute about 34% of the cross section area. This was the justification for the addition of hollow specimens for comparison purposes.

This non-uniformity makes the exact numerical values have less meaning in a practical application. For example, it would be unwise to model infill in a part as a uniform material having the exact stiffness as described and relying on deformation data from a computer load simulation of said part. However, when designing you could use infill as a way to stiffen up your initially hollow part without adding too much mass. The

data shows stiffness of specimens with infill as being significantly larger than those without infill.

Improvements which could be made to the experiment and ideas for future testing

1. Significantly reducing print errors

This could be done by using a higher grade printer than the desktop printer used to print the samples tested in this experiment. A higher grade printer would have better resolution to print the finer details of the infill more precisely and would be less prone to plastic buildup on the nozzle which frequently gets stuck to the parts. Large plastic globules, which were unintentionally stuck to the test specimens, frequently had to be sanded off in order to perform the testing which affected the material properties of the specimens. If the specimen volumes were identical, the strength comparisons could be done with ultimate tensile strength versus mass which would be better representations of the material properties.

2. Increasing infill percentage and minimizing exterior wall thickness

Increasing the infill percentage would minimize the infill geometry size and reducing the wall size would reduce the contribution of the wall to the strength of the test specimen. Both increasing infill percentage and minimizing exterior wall thickness would increase the uniformity of the test specimen and lead to more accurate results which would better reflect the properties of the infill.

3. Making the ends of the test specimens solid

Making the volume of the test specimens outside the gauge length solid (as done for the finite element testing) would eliminate failure outside of gauge length as solid material is far stronger than infill material. The finite element analysis showed that the solid material outside the gauge length had significantly lower stress than material along the gauge length (note the color differences in figures 11, 13, and 15 indicating lower stresses present outside the gauge length). The problem with this is that it would be difficult and time consuming to program a 3D printer to have different infill rules for certain areas. One would have to either CAD samples with infill only along the gauge length or try to modify the slicing program.

4. Reduce number of variables or add more samples or both

Very few tests were performed while many variables were modified. If there were more than one test for a particular set of parameters, the tests could be averaged and the precision could be checked. Also having more variation on one variable

would give a better picture of the effect of that variable on the stiffness and strength of the infill material.

5. Including more materials or infill styles

This would increase the scope of the experiment and provide more guidelines for designers. New infill styles could be tested to see if they are better than the preexisting ones. For example, slic3er has developed a new 3D honeycomb infill. The goal of this infill is to have strength properties that are independent of orientation. Testing of this infill would be very informative.

6. Varying infill geometry wall thickness while holding infill percentage, geometry, and orientation constant.

7. Testing the various part parameters in a compression test.

Solid 3D printed material has been shown to be stronger in compression. [9] Whether the same is true for material with infill could be an avenue for experimentation.

Design Considerations for 3D Printed Parts

- Hexagonal Infill was found to be stronger and stiffer than rectangular infill
- As material is removed, the strength to mass ratio decreases.
- Printing difficulty

Many possible samples were not tested because the desktop printer had difficulty producing them. As a general rule, parts should be printed with their shortest dimension in the vertical direction. [3] This makes it easier to print and generally minimizes the amount of support material. Other studies [3] note that solid test specimens were stronger when printed with their shortest dimension aligned with the vertical/print axis. (Stiffness was not significantly affected by print direction).

- Choice of infill geometry shape, infill percentage, and slicing program.

If the size of the infill geometry is comparable with the smaller dimensions in the design, irregularities in the properties of the object may occur. For example, Sample 12 fractured outside the gauge length because the infill geometry size was comparable to the width of the test specimen leading to an unanticipated weakness in its structure. This would have been

avoided with a larger infill percentage which would lead to smaller infill.

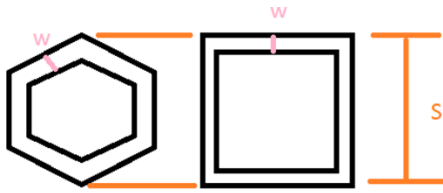


Figure 18: Infill geometry with the dimensions which define it assuming shape is predefined.

The size of infill geometry (dimension “S” in the figure) is defined both by infill percentage and infill wall thickness. (Dimension “W” in the figure) Some slicing programs (a program which converts a CAD model into GCODE which tells the printer how to print the part) assign larger wall thicknesses for infill geometry. For a fixed infill percentage “S” and “W” are directly proportional, so increasing “W” by a factor increases the size of the infill geometry by the same factor.

Hexagonal geometry is much larger than rectilinear geometry. For parts where hexagonal geometry may be too big at a fixed percentage, rectilinear geometry could be used at the same percentage and could lead to more uniform properties.

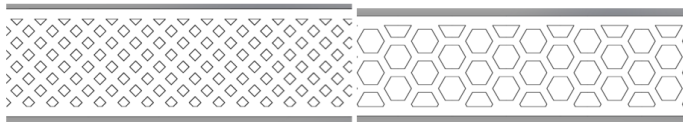


Figure 19: CAD model of two test specimens used in finite element analysis. Both have identical exterior wall thicknesses, infill wall thicknesses, and infill percentages. The hexagons are much larger.

CONCLUSIONS

This experiment examined the variations in mechanical properties of 3D printed material due to a variety of factors. It is clear that further study of the trends proposed by this study is necessary due to the limited number and limited quality of samples it used to provide these results. Also, the discrepancies between the finite element results and the experimental data suggest that stress concentrations may have caused samples to fail prematurely. There are so many factors that need to be analyzed when it comes to predicting the strength of 3D printed parts. As 3D printing becomes more mainstream, companies will want to know how to maximize the strength and durability of the products they print. With more attention being brought to additive manufacturing, UC Berkeley has an opportunity to prepare their students with key skills which will be required for the jobs of tomorrow by being experts in additive manufacturing. The mechanics of engineering materials class (ME 108) is well suited to examine these topics in their their labs. This experiment could serve as a template for a new lab for that class and could lay the foundation for the introduction of 3D printing material

and manufacturing processes to become a part of the ME 108 curriculum. The data and resulting guidelines may also be incorporated into UC Berkeley’s ME 220 Precision Manufacturing course in the section--under development--precision digital fabrication.

The engineering students of UC Berkeley are the designers and manufacturers of tomorrow. 3-D printing is already growing at a fast pace and this experiment has the potential to integrate this increasingly important manufacturing process into the UC Berkeley mechanical engineering education, giving students the tools and information necessary to design lighter, stronger, better and more affordable products that could have a profound impact on society.

ACKNOWLEDGMENTS

The authors would like to thank you3Dit for providing funding for this experiment as well as the UC Berkeley Mechanical Engineering department and the machine shop staff for allowing them to use the testing equipment.

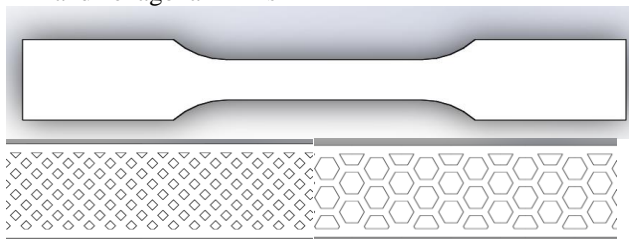
REFERENCES

1. "ABS vs PLA." *BotFeeder*. BotFeeder, 02 Oct. 2013. Web. 02 Aug. 2015.
2. Anisotropic material properties of fused deposition modeling ABS
Sung- Hoon Ahn, Michael Montero, Dan Odell, Shad Roundy, Paul K. Wright
Rapid Prototyping Journal 2002 8:4 , 248-257
3. Barclift, M., & Williams, C. (2012). Examining Variability in the Mechanical Properties of Parts Manufactured Via Polyjet Direct 3D Printing. Retrieved September 7, 2015.
4. D’Aveni, Richard. "The 3-D Printing Revolution." *Harvard Business Review* May (2015): 40-48. Print.
5. K. Komvopoulos, *Mechanical Testing of Engineering Materials*, (USA: University Readers, Inc., 2011).
6. 3D Printing a 3D Honeycomb Infill concept. (2015, July 24). Retrieved September 18, 2015, from <http://engineerdog.com/2015/03/08/3d-printing-a-3d-honeycomb-infill-concept/>
7. Mechanical Testing 3D Printed Parts: Results and Recommendations. (2015, September 2). Retrieved September 18, 2015, from <http://engineerdog.com/2015/09/02/mechanical-testing-3d-printed-parts-results-and-recommendations/>
8. 3D Printing Infill. (2014). Retrieved September 18, 2015, from <http://triplaxis.deviantart.com/art/3D-Printing-Infill-433183209>
9. Wright, P., Ahn, S., Montero, M., Odell, D., & Roundy, S. (2002). Anisotropic Properties of Fused Deposition Modeling. *Rapid Prototyping Journal*, 2002(8), 248-248. Retrieved September 30, 2015, from <http://www.ewp.rpi.edu/hartford/~sayer/Master's Project/other/Research/Anisotropic material properties of fused deposition modeling.pdf>

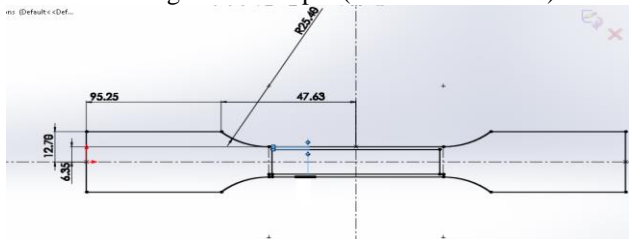
ANNEX

ADDITIONAL EXPERIMENTAL INFORMATION

1. Image of solid model and section views of rectilinear and hexagonal infills



2. 2D drawing of test sample (dimensions in mm)



3. Device used to measure mass of samples: Adventurer Pro is a device intended to give precise mass measurements for chemistry experiments. Use of this device allowed for highly accurate and precise measure of the mass of each sample. This measurement was performed after fracture which is not ideal due to loss of material. However, this loss would be small in comparison to the total mass of the specimen.

